IEEE Robotics and Automation Letters (RAL) paper presented at
2024 IEEE/RSJ International Conference on Intelligent Robots and Systems (IROS)
October 14-18, 2024. Abu Dhabi, UAE

Assessment and Modeling of the Aerodynamic Ground Effect of a Fully-Actuated Hexarotor With Tilted Propellers

Ambar Garofano-Soldado, Antonio Gonzalez-Morgado, Guillermo Heredia, *Member, IEEE*, and Anibal Ollero, *Fellow, IEEE*

***Abstract*—This letter investigates the ground proximity effects of a fully-actuated multirotor unmanned aerial vehicle (UAV). Different configurations of tilted rotors and a wide range of UAV heights relative to the ground are considered. In order to characterize the effect, an extensive experimental study was conducted on a static test-bench. The experimental results display a behavior differing from that previously observed for multirotors with co-planar propellers and single-tilted rotors. We demonstrate that the ground effect increases with angle when the UAV is near the ground, while the opposite occurs for areas further away. Two new ground effect models are proposed, one for co-planar and another for fully-actuated configuration. In both cases, the models are dependent on the propeller radius, the distance between the rotors, the height of the UAV and the fountain effect. In addition, in the fully-actuated configuration, the model also depends on the inclination of the rotors. Finally, the proposed models are integrated into the UAV control architecture using the Aerodynamic Power Model Inversion (APMI) module, showing a significant improvement in flight accuracy when the ground effect is considered.**

***Index Terms*—Aerial robot, ground effect, fully-actuated, aerodynamics, tilted rotors.**

I. Introduction

THE range of applications for multirotor unmanned aerial vehicles (UAVs) has expanded in recent decades due to their ability to perform tasks in multiple fields [1]. In particular, there is growing interest in using aerial robots for infrastructure inspection and maintenance [2], [3], [4]. These tasks involve direct contact between the UAV and the environment [5], aerial manipulation tasks [6] or flying close to surfaces or objects, often posing a risk to people.

Multirotors with co-planar propellers are widely used because of their low cost, mechanical simplicity, and ease of control. Much work has therefore focused on modeling, controlling, and designing different configurations of conventional multirotors [7]. However, these aerial robots can only generate thrust in one direction and must incline to move in the horizontal plane. This manoeuvre is not very efficient, as it increases the effective surface area and therefore the aerodynamic drag when moving sideways. In such cases, roll and pitch motions are required for translational motion, resulting in a loss of controllable degrees of freedom. This inherent under-actuation has led to multirotor with tilted propellers becoming increasingly common for tasks which require high precision. Fully-actuated aerial platforms are optimal candidates for working in narrow, high or hard-to-reach areas as the horizontal component of the force prevents the UAV from having to tilt to move [8], [9], [10]. In this way, safer and more stable flights are achieved when contact is necessary or proximity to surfaces is required [11].

The operation of UAVs in confined environments leads to the occurrence of various aerodynamic effects that alter the performance of the aerial vehicle. The propeller's flow is constrained by the presence of a surface such as a ground, wall or ceiling, making it unable to develop freely. Although several works have examined different aerodynamic effects in the vicinity of surfaces using multirotors with co-planar propellers [8], [12], [13], [14], [15], very few have focused on fully-actuated platforms [16], [17], [18]. Therefore, this letter aims to provide a better understanding of the ground effect on fully-actuated aerial platforms.

The ground effect refers to the increase in thrust experienced by a rotor/UAV when it is close to the ground. Exploiting this effect would mean that the motors would need less thrust and could fly at lower power. However, it is necessary to characterize the ground effect beforehand to incorporate it into a controller capable of anticipating. In this way, the effect would be exploited while avoiding platform instability. Initially, the ground effect was studied in helicopters with a single propeller. Although several models were developed, the Cheeseman and Bennet theory is the most widely used [19]. Later, the ground effect was studied in multirotor with co-planar propellers. Several works have shown that the interaction between the propeller flows has an important effect on the ground effect and that single propeller models cannot be used [12], [14], [15]. A literature review on ground effect models for co-planar rotors is given in [20]. However,

Manuscript received 30 July 2023; accepted 21 December 2023. Date of publication 8 January 2024; date of current version 17 January 2024. This letter was recommended for publication by Associate Editor Krishnanand N. Kaipa and Editor L. Pallottino upon evaluation of the reviewers' comments. This work was supported in part by MARTIN Project under Grant PID2022-143267OB-I00, funded by MCIN/AEI/10.13039/501100011033 and ERDF A Way of Making Europe, in part by AEROTRAIN Marie Sklodowska-Curie under Grant MSCA-ITN-2020-953454, in part by H2020 PILOTING under Grant H2020-ICT-2018-871542, in part by H2020 AERIAL-CORE under Grant H2020-2019-871479, and in part by SIMAR under Grant HE-CL4-2021-101070604 Projects, funded by the European Union. The work of Ambar Garofano-Soldado was supported by the FPI under Grant PRE2019-089812 from the Ministry of Science and Innovation of the Spanish Government. *(Corresponding author: Ambar Garofano-Soldado.)*

The authors are with GRVC Lab, Department of Systems Engineering and Automatics, University of Seville, 41092 Seville, Spain (e-mail: agarofano@us.es; mantonio@us.es; guiller@us.es; aollero@us.es).

This letter has supplementary downloadable material available at https://doi.org/10.1109/LRA.2024.3350975, provided by the authors.

Digital Object Identifier 10.1109/LRA.2024.3350975

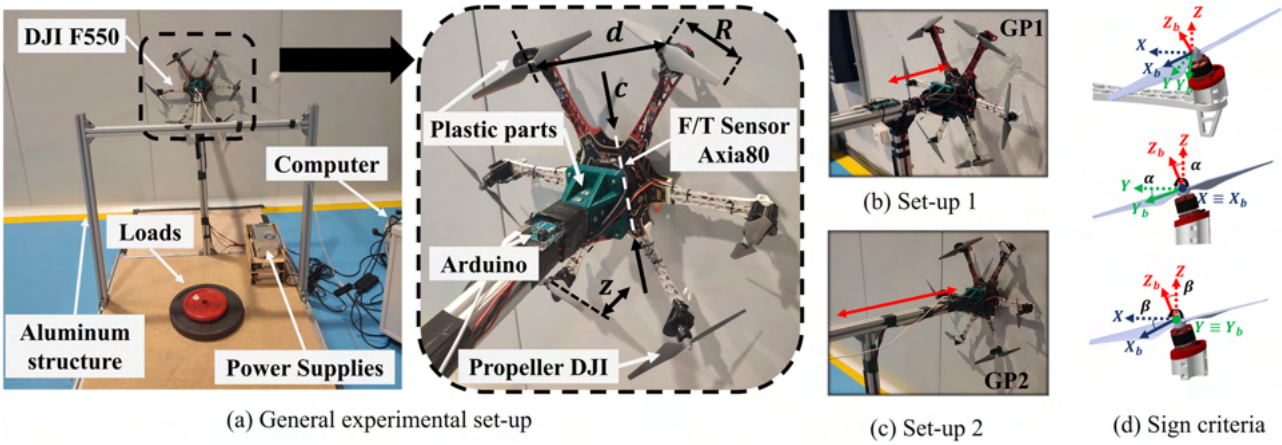

Fig. 1. Test-bench to characterize the ground effect of a hexarotor with tilted rotors. In (a), the complete test-bench is illustrated, where the aluminum structure will be moved to take measurements at each height (z). In addition, an enlarged image of the UAV with the parameters of interest is shown. In (b) and (c) the two tested test-bench configurations and two different types of ground plane (GP1 and GP2) are shown. The sign criterion considered in the positioning of the motors is given in (d).

multirotors with inclined propellers have been the subject of less research due to their novel concept. Along these lines, the ground effect of a single-tilted rotor is examined in [21]. In addition, a model is proposed in which the thrust increase depends on both the rotor height and the rotor inclination. However, this model could not be used for full multirotors with tilted propellers as it does not consider the influence of adjacent rotors. Unlike co-planar configurations, fully-actuated platforms typically have two different pairs of rotors: Face-to-Face (F-F), where the flows do not intersect, and Back-to-Back, where the flows overlap [17]. For this reason, each pair of rotors near the ground was analyzed in [18] and two aerodynamic models were proposed. The ground effect was shown to be different for each configuration (F-F and B-B). However, due to the simultaneous presence of the F-F and B-B pairs in a fully-actuated hexarotor, these models are not directly applicable to a full multirotor. Other models for aerial vehicles with tilted rotors have been developed without consideration of surface interactions [16]. Given that the behavior of fully-actuated multirotors differs from that of conventional multirotors, it is necessary to study and model the ground effect in this new configuration. To fill this gap in the literature, this letter evaluates the ground effect on a fully-actuated aerial platform using a static bench test. Rotor inclinations between $10^\circ - 30^\circ$ and ten heights (z) of the UAV relative to the ground are under consideration. The aim is to improve understanding of how proximity affects platforms with tilted rotors. In addition, the first ground effect model for a fully-actuated multirotor is proposed. To this end, a semi-empirical model is first obtained for the co-planar configuration and then extended to include the inclination. Finally, the validation of the proposed ground effect models is carried out on real indoor flights.

The remainder of the letter is organized as follows. Section II describes the test-bench designed to characterize the ground effect at different rotor inclinations. In addition, the experimental results are presented and compared with previous theories. Section III details the aerodynamic models developed for the co-planar and tilted case. Section IV is devoted to the experimental validation of the ground effect models by means of real indoor flights. Finally, Section V draws conclusions.

II. Data Acquisition and Analysis

A. Test-Bench

Fig. 1(a) shows the test-bench developed to investigate the ground effect on a hexarotor platform with tilted propellers. Initially, the tests were performed with set-up 1 (see Fig. 1(b)), where the wall is rough and made of concrete. Also, the distance between the UAV and the vertical aluminium bar is small. Then, in set-up 2 (see Fig. 1(c)), the test-bench was modified to separate the UAV from the aluminium structure. This was done to prevent the flow returning from the impact with the ground from interfering with the structure. In this case, the wall is made of plastic. In any case, an aluminium frame with the dimensions $1 \times 1 \times 1$ (m) was built to fix the aerial platform. The experiments were performed using a DJI F550 hexarotor with six DJI E310 2312 motors and six DJI 9.4'$\times$5' propellers. An ATI 6-DoF (degree of freedom) force/torque sensor was placed between the aluminium frame and the UAV to measure the total force exerted by the aerial platform at different distances from the wall (z). This sensor was located in the centre of the DJI chassis.

Several plastic parts were designed and manufactured to ensure the inclination of the motor-propeller assembly and to attach the UAV and sensor to the aluminum structure. Each motor requires two different parts to tilt it into the desired position. It is worth noting that these parts were designed according to [4] and with two objectives in mind: a) minimum height to reduce weight and avoid the motor being too far from the UAV arm, b) to avoid the propeller intersecting with the UAV. The motors have two inclinations: cant angle α, which is the rotation relative to the X-axis, and dihedral angle β, which is the rotation with respect to the Y-axis [16]. The sign criterion is the same as that proposed by [22] (see Fig. 1(d)). In this study, $\alpha = \beta$ is considered for the sake of simplicity and because it is the setting used in previous work [4].

The velocity of the motors is controlled by an Arduino Mega and set to 5000 rpm. This velocity is within the $50 - 60\%$ throttle range, which is commonly employed in UAVs. Furthermore, it is constant and fixed for all motors. Four power supplies are

TABLE I
DEFINITION OF THE UAV PARAMETERS, THE INCLINATIONS AND HEIGHTS TO BE TAKEN INTO ACCOUNT FOR GROUND PROXIMITY ASSESSMENT

Parameter	Description	Value
R	Propeller radius	0.1194 [m]
c	Frame width	0.22 [m]
d	Propeller spacing	0.28 [m]
α, β	Inclination angles	$0°$, $10°$, $20°$, $30°$
z/R	Nondimensional distance	$1.1, 1.5, 2, 2.5, 3, 4, 5, 6, 7, 8$

utilized, one for each of the two motors and one for the sensor to provide a constant voltage.

Experiments were carried out for ten different distances from the wall (z) and four configurations of α, β. The distance z is measured from the propeller centre of rotation to the wall (or ground). A total of 60 experiments were performed to assess the ground effect of the hexarotor. In each experiment, five tests were run to obtain an average value of the total force for the chosen configuration z, $\alpha = \beta$. Table I summarises the parameters and working conditions of the experiments. Each test has a total duration of 90 seconds and consists of four phases: 1) 20 seconds where the motor is turned off, 2) the following 10 seconds, the motor has a speed between $10 - 40\%$ throttle, 3) 20 seconds in which the motor has a constant speed between $50 - 60\%$ throttle and 4) the motor speed is reduced to a minimum for 40 seconds to help stabilise the motor temperature before the next test [23]. Stage 2 prevents voltage peaks in the motor, and stage 3 allows the data of interest to be collected.

B. Experimental Analysis

Ground effect is usually represented by the ratio T_{IGE}/T_{OGE}, where T_{IGE} is the thrust of the rotor/UAV in the presence of the ground (In-Ground-Effect), and T_{OGE} is the thrust of the rotor/UAV when it is sufficiently far from the ground (Out-of-Ground-Effect) [20]. This ratio quantifies the increase in thrust experienced by the rotor/UAV as it approaches the ground.

Fig. 2 illustrates the experimental data for the hexarotor when $\alpha = \beta = 0°$ in red dashed line. The results are also compared with various ground effect models developed in the past [20]. On the one hand, the experimental data are benchmarked against the models derived for a complete multirotor. On the other hand, the upper right-hand side of Fig. 2 displays in shading the comparison of the hexarotor experimental results with ground effect models for a single-rotor. It is observed that the thrust ratio (T_{IGE}/T_{OGE}) is significantly more noticeable in the case of a multirotor than in the single-rotor configuration. The deviations between the experimental data and the other models are remarkable. The Sanchez-Cuevas et al. model is the closest to the behavior of the hexarotor. However, the discrepancies are evident when the UAV is very close to the ground. Here, the errors found are around 15%. As the distances closest to the ground are the most critical, a model that accurately captures the thrust increase of a co-planar hexarotor is required. Fig. 2 shows that none of the previously developed models can be directly applied to the configuration analyzed in this letter. Therefore, a new ground effect model must be defined that accurately fits the behavior of a co-planar hexarotor.

Fig. 3 shows the experimental results of the ground effect for $\alpha = \beta = 10°, 20°$ with two different set-ups. In any case, the results achieved are practically the same. This demonstrates the robustness of the test-bench and the independence of the wall

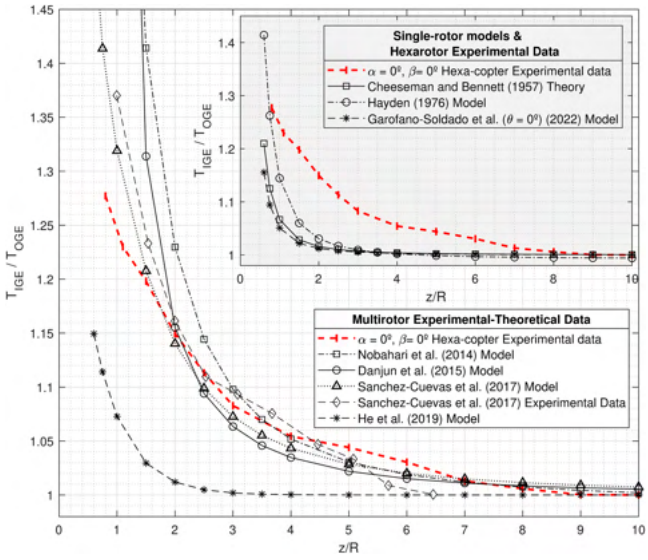

Fig. 2. Thrust ratio (T_{IGE}/T_{OGE}) versus dimensionless height z/R. Comparison of experimental measurements of the co-planar propeller hexarotor with previous theories developed for multirotors. In the shaded area, the experimental measurements of the UAV are contrasted with previous models of the isolated rotor.

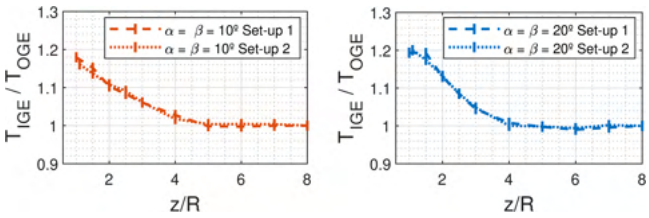

Fig. 3. Experimental results of the thrust increase experienced by the hexcopter with inclined propellers on different test-benches. Two types of ground were considered and the inclination $\alpha = \beta = 10°, 20°$ was used.

type in the ground effect analysis. Similarly, the thrust ratio was determined for $\alpha = \beta = 30°$. Fig. 4 plots all the experimental results for the inclined case. Several trends are identified in a hexarotor with tilted propellers. On the one hand, from $1R$ to $2R$ the ground effect is found to increase with α, β. On the other hand, from about $2.5R$ onwards, the trend is reversed and the ratio T_{IGE}/T_{OGE} decreases with angle. Previous theories do not consider the tilt angle of the rotors in a multirotor. However, the first ground effect model was proposed in [21] for single-tilted rotors. On the one hand, in the upper right-hand side of the Fig. 4, it is shown in shading how the thrust ratio changes when an isolated propeller is tilted with respect to the ground (θ). Ground effect reduces with angle (θ). On the other hand, the experimental results are compared with the models proposed in [18] for the two pairs of rotors typically found in a fully-actuated hexarotor: Face to Face (F-F) and Back to Back (B-B) [17]. It is worth noting that the ground effect increases with the inclination for the B-B pair, while the opposite trend occurs for the F-F pair. In addition, for the same inclination, the B-B pair has a greater effect. These two configurations are present simultaneously in a complete fully-actuated hexarotor, giving rise to two opposite trends. However, it is not possible to use the single or two-rotor models in this configuration, as the ground

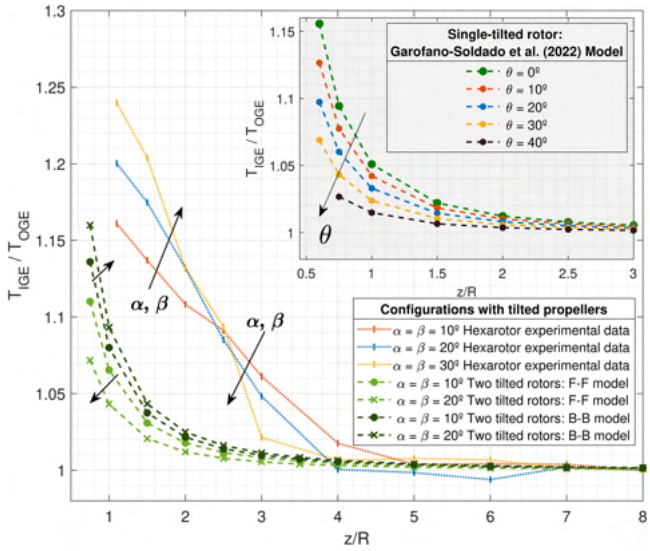

Fig. 4. Thrust ratio versus non-dimensional distance z/R for different rotor inclinations. The results are obtained experimentally for a fully-actuated hexarotor and are compared with the proposed models for the two pairs of rotors F-F and B-B. The shaded area shows the single-inclined rotor model. Several trends and a transition zone are identified.

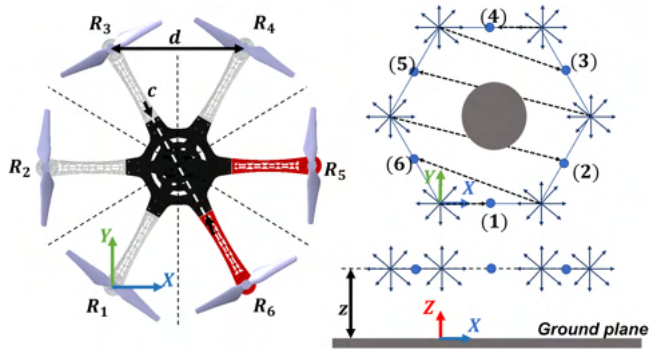

Fig. 5. Schematic to detail the considerations taken to derive the ground effect model of a hex-copter. The layout of the rotors and the positioning of the potential sources are displayed. The blue circle represents the zone of greatest interference between two propellers, corresponding to the interaction of the blade tip vortices.

effect is increased by the fountain effect and the interaction between the propellers. In addition, the previous models shown in Fig. 2 cannot be considered in a fully-actuated platform, as they do not take into account the inclination of the propellers. The dual inclination and the two-rotor configurations that exist in a fully-actuated platform cause the ground effect results to have a varying tendency.

III. Aerodynamic Ground Effect Modelling

This section presents the aerodynamic ground effect model developed for a hexarotor with tilted propellers. First, a model is proposed for the case where the propeller plane is parallel to the ground. Next, based on this model, the angle of inclination of the propeller is included. Finally, the proposed models are validated with experimental data collected on the test-bench.

A. Co-Planar Configuration

A model for a hexarotor with co-planar propellers is derived from the theory of Cheeseman and Bennett, which is the most commonly used for both small and large-scale propellers [19]. This theory is based on considering the rotor as a 3D potential source. After applying the method of images and considering constant power ($T_{IGE} \cdot v_{i_{IGE}} = T_{OGE} \cdot v_{i_{OGE}}$), it is found: $T_{IGE}/T_{OGE} = 1/(1 - \delta v_i/v_{i\infty}) = 1/(1 - (R/4z)^2)$, where R is the propeller radius, $\delta v_i(z)$ is the velocity induced resulting from the rotor image at a distance of $(0, 0, -z)$ and $v_{i\infty}$ is the velocity induced of the rotor when the ground surface is non-existent ($v_{i\infty} = v_{i_{OGE}}$). Moreover, $v_{i_{IGE}}$ is the velocity induced below ground and it is defined as: $v_{i_{IGE}} = v_{i_{OGE}} - \delta v_i$.

In the hexarotor configuration, the classical Cheeseman and Bennett theory is extended and each rotor is treated as a potential source. In addition, the method of images is used to set the ground boundary condition. The presence of the image reduces the induced velocity of the individual rotor in a similar way to what would happen at ground level. It should be noted that the definition of a 3D potential source is: $\phi(x, y, z) = s/(\sqrt{(x - x_0)^2 + (y - y_0)^2 + (z - z_0)^2})$, in which s is the source strength, and (x_0, y_0, z_0) is the rotor position (or source). The strength of the sources is established as $s = A v_{i_\infty}/4\pi$ according to [19]. The induced velocity (δv_{i_n}) is specified for each rotor, where n is the number of rotors ($n = 1, \ldots, 6$). Under these considerations, it comes to:

$$\delta v_{i_1}(z) = \frac{R^2}{2} \cdot \frac{z v_{i_{OGE}}}{\left[x_1^2 + y_1^2 + 4z^2\right]^{\frac{3}{2}}}, \tag{1}$$

$$\delta v_{i_2}(z) = \frac{R^2}{2} \cdot \frac{z v_{i_{OGE}}}{\left[(x_2 + d/2)^2 + \left(y_2 - \frac{\sqrt{3}}{2}d\right)^2 + 4z^2\right]^{\frac{3}{2}}}, \tag{2}$$

$$\delta v_{i_3}(z) = \frac{R^2}{2} \cdot \frac{z v_{i_{OGE}}}{\left[x_3^2 + (y_3 - \sqrt{3}d)^2 + 4z^2\right]^{\frac{3}{2}}}, \tag{3}$$

$$\delta v_{i_4}(z) = \frac{R^2}{2} \cdot \frac{z v_{i_{OGE}}}{\left[(x_4 - d)^2 + (y_4 - \sqrt{3}d)^2 + 4z^2\right]^{\frac{3}{2}}}, \tag{4}$$

$$\delta v_{i_5}(z) = \frac{R^2}{2} \cdot \frac{z v_{i_{OGE}}}{\left[\left(x_5 - \frac{3}{2}d\right)^2 + \left(y_5 - \frac{\sqrt{3}}{2}d\right)^2 + 4z^2\right]^{\frac{3}{2}}}, \tag{5}$$

$$\delta v_{i_6}(z) = \frac{R^2}{2} \cdot \frac{z v_{i_{OGE}}}{\left[(x_6 - d)^2 + y_6^2 + 4z^2\right]^{\frac{3}{2}}}. \tag{6}$$

In this case, $v_{i_{OGE}} = v_{i_\infty}$ and $x_n - y_n$ coordinates must be determined. Moreover, the superposition principle is applied to consider the six rotors, where the linear addition of different flows is done. This allows more complex flows to be generated. Fig. 5 shows the arrangement of the rotors and the parameters of interest. The general formulation of the ground effect model

for the co-planar configuration is as follows:

$$\left[\frac{T_{IGE}}{T_{OGE}}\right]_{(z)} = \frac{1}{1-\sum_{n=1}^{6}\left(\frac{\delta v_{i_n}}{v_{i_\infty}}\right)_{R_n} - \triangle\, v_{i_f}(z)}. \quad (7)$$

The term $\triangle\, v_{i_f}(z)$ must be included to account for the fountain effect in the UAV body. As discussed in [15], a recirculating flow appears below the central frame, pushing the UAV upwards. Sanchez-Cuevas et al. looked at the air velocity at the centre of the multirotor and adjusted the J_k term by experimental measurements leading to:

$$\triangle\, v_{i_f}(z) = \frac{2R^2 J_k}{[r_d^2 + 4z^2]^{\frac{3}{2}}} z. \quad (8)$$

Considering that the interaction of opposing rotors flows is mainly responsible for the fountain effect, it is assumed that $r_d = 2d - c$, where c is the width of the central frame and $2\,d$ is the distance between two opposite rotors, as shown in Fig. 5. Also, J_k is adjusted with co-planar hexarotor experimental data by taking a value of $J_k = 2.2$. In order to achieve an expression that depends only on the propeller radius (R), the rotor spacing (d) and the ground clearance (z), additional considerations need to be taken into account.

Assumption 1: The mid-position between two propellers is where maximum interference occurs. The blade tip vortices of both propellers interact with each other and with the ground. This location is marked with a blue circle between two sources in Fig. 5.

Assumption 2: As the fountain effect arises from the combination of opposing flows, the mid-points are enumerated in the reverse direction to the rotors, as seen in Fig. 5. Arrows indicate direction from the rotor (R_n) to its corresponding centre point (x_n, y_n). Flows from different rotors do not cross each other, but contribute to the flow passing under the central frame pushing it upwards.

Hence, the co-planar hexarotor ground effect model becomes:

$$\left[\frac{T_{IGE}}{T_{OGE}}\right] = \frac{1}{1 - \frac{R^2\cdot z}{[d^2/4+4z^2]^{\frac{3}{2}}} - \frac{R^2}{2}\cdot\frac{z}{\left[\frac{21\,d^2}{4}+4z^2\right]^{\frac{3}{2}}} - \frac{1}{-\frac{R^2\cdot z}{\left[\frac{13\,d^2}{4}+4z^2\right]^{\frac{3}{2}}} - \frac{R^2}{2}\cdot\frac{z}{\left[\frac{7\,d^2}{4}+4z^2\right]^{\frac{3}{2}}} - \frac{2R^2 z J_k}{[r_d^2+4z^2]^{\frac{3}{2}}}}}. \quad (9)$$

This model will be used as a starting point for considering the inclination of the rotors in a similar way to that in [21].

B. Tilted Configuration

The ground proximity effect differs between co-planar and tilted propeller aerial platforms (see Figs. 2 and 4). Therefore, a new ground effect model is proposed that takes into account the inclination of the rotors. In Fig. 4 three main sections can be distinguished: 1) up to 2.5 R, there is an upward trend with α and β, 2) between 2.5 R and 3 R there is a crossing of curves, and 3) from 3 R onwards, the ground effect decreases with angles α, β. For this reason, a piecewise-defined model is presented.

TABLE II
NON-DIMENSIONAL COEFFICIENTS USED IN THE DEFINITION OF INDUCED VELOCITY OUT OF THE GROUND EFFECT IN SECTIONS 1 AND 3 OF FIG. 4

Section	K_c	K_j	K_h
1	m_0	$m_1 sin(\beta)$	$m_2 cos(\beta)$
3	n_0	$n_1 sin(\beta)$	$n_2 cos(\beta)$

TABLE III
VALUES OF THE VARIABLES INVOLVED IN THE HEXAROTOR GROUND EFFECT MODELS WITH INCLINED PROPELLERS DETERMINED FROM EXPERIMENTAL MEASUREMENTS

Section 1		Section 2 (A)		Section 2 (B)		Section 3	
Parameter	Value	Parameter	Value	Parameter	Value	Parameter	Value
m_0	0.216	d_0	-0.0136	r_0	1.105	n_0	0.553
m_1	0.841	d_1	-0.1994	r_1	0.706	n_1	-8.784
m_2	0.826	d_2	-0.1851	r_2	0.329	n_2	4.874

In sections where there is an upward or downward trend in the ground effect with angle (sections 1 and 3), the co-planar hexarotor model is extended to include α and β in a similar way to [18]. However, at $2.5\,R$ the curves intersect and it will be necessary to model this point of trend change in a different way. Consequently, between $2.5\,R$ and $3\,R$ (section 2), a linear approximation is used to model the transition between section 1 and section 3.

As in [21], δv_{i_n} is taken to depend on both (z) and angle (α, β), and the induced velocity away from the ground ($v_{i_{OGE}}$) is written as:

$$v_{i_{OGE}} = v_{i_\infty} f_t(\alpha,\beta) = v_{i\infty}(K_c + K_j\cos(\alpha) + K_h\sin(\alpha)), \quad (10)$$

where K_c, K_j and K_h are non-dimensional coefficients to be determined for each section (see Table II). Equation (10) is applied in sections 1 and 3 as Fig. 4 shows similar trends to [18]. This indicates that assumptions can be made based on the change in induced velocity with inclination. However, the transition area, where the trend changes, must be modelled separately. The Levenberg-Marquardt algorithm was used to find the values of the variables $m_0, m_1, m_2, n_0, n_1, n_2$ (see Table III).

In general, in section 1 and 3, the ground effect model for a hexarotor with tilted propellers is as follows:

$$\left[\frac{T_{IGE}}{T_{OGE}}\right]_{(z,\alpha,\beta)} = \frac{1}{1-\sum_{n=1}^{6}\left(\frac{\delta v_{i_n}}{v_{i_\infty}}\right)_{R_n} f_t(\alpha,\beta) - \triangle\, v_{i_f}(z)}. \quad (11)$$

In contrast, a linear model is proposed for the transition zone (section 2):

$$\left[\frac{T_{IGE}}{T_{OGE}}\right]_{(z_2)} = A\cdot\left(\frac{z}{R}\right) + B. \quad (12)$$

The coefficients A and B are defined as set out below:

$$A = [d_0 + d_1\cos(\alpha)\sin(\beta) + d_2\sin(\alpha)\cos(\beta)],$$
$$B = [r_0 + r_1\cos(\alpha)\sin(\beta) + r_2\sin(\alpha)\cos(\beta)], \quad (13)$$

where $d_0, d_1, d_2, r_0, r_1, r_2$ are variables to be determined from the experimental data by means of least square fitting. The values of these variables are given in Table III.

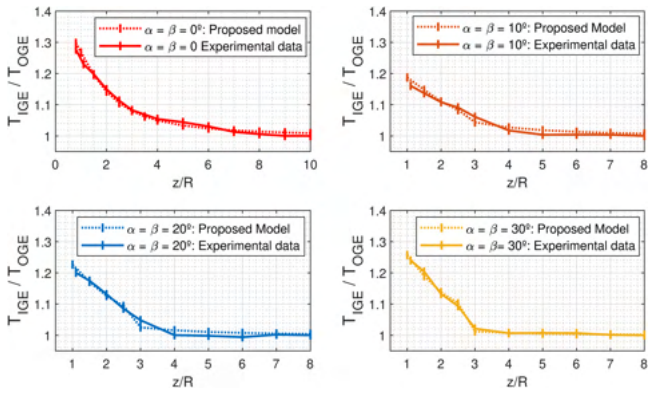

Fig. 6. Comparison of the experimental thrust ratio (solid line) and that obtained with the proposed models (dot line). A good fit and an improvement over previous theories can be seen.

C. Evaluation of Proposed Models

Fig. 6 shows the variation of the thrust ratio with the nondimensional height (z/R) from both experimental measurements and proposed models in the co-planar and tilted configuration. A good agreement between the experimental results and the different semi-empirical models is found. This suggests that both the assumptions and the estimates made in each section adequately capture the trend in the ground effect.

The models presented in this section for both the co-planar and inclined configurations are applicable under static conditions as forward velocity is not considered in this study. Therefore, external environmental factors such as wind are not taken into account. Previous work has examined the ground effect of co-planar platforms at different forward velocities and found that the ground effect decreases as the velocity increases [14]. However, at high velocities, the effect increases and then decreases again. In any case, the thrust increase experienced by the UAV at zero or very low velocity is still higher than in the other cases. Accordingly, this letter would deal with the worst case.

The performance of a propeller depends on the Reynolds number [24]. Small-scale propellers will have a lower Reynolds number than large-scale propellers used in helicopters or large UAVs. The proposed models can only be used on small-scale propellers with low Reynolds numbers. In addition, the propeller tilt should not exceed 30° as higher values have not been tested.

IV. Experimental Validation

This section presents the validation of the proposed models in real indoor flights for the co-planar configuration and for the fully-actuated configuration. These models have been incorporated in the control architecture of both configurations.

A. Control Architecture

The control architecture of multirotors is composed of the position controller, which controls the position $\boldsymbol{p} = [x,\ y,\ z]$ and the attitude controller, which controls the Euler angles $\boldsymbol{\eta} = [\phi,\ \theta,\ \psi]$. For conventional multirotors with co-planar propellers, these controllers are coupled, as the position controller modifies the roll and pitch angles references to move in the XY plane. To control the platform, the position controller commands a force $\boldsymbol{F_C} = [F_X,\ F_Y,\ F_Z]$, while the attitude controller commands a torque $\boldsymbol{\tau_C} = [\tau_X,\ \tau_Y,\ \tau_Z]$. In the case of the co-planar configuration, where controllers are coupled, the roll and pitch references are created using the yaw reference and the commanded force $\boldsymbol{F_C}$, as shown in Fig. 7(a). However, for fully-actuated platforms, these controllers are decoupled, as the 6DoF can be controlled independently, as Fig. 7(b) illustrates. For this case, the force $\boldsymbol{F_C}$ and torque $\boldsymbol{\tau_C}$ are directly commanded to the motors using the mixer, which depends on the tilted angles α and β. For more information about fully-actuated platforms, refer to [4], [10].

The proposed models presented in Section III have been incorporated into the UAV controller to correct the ground effect through the Aerodynamic Power Model Inversion (APMI) module. For doing that, the output F_Z from the position controller is corrected with the model presented in Section III-A (co-planar configuration) and III-B (tilted configuration). The corrected control force would be $\widehat{F_Z} = F_Z/K_{IGE}(z,\alpha,\beta)$, where $K_{IGE}(z,\alpha,\beta) = T_{IGE}/T_{OGE}$ is the thrust ratio that represents the ground effect. Without the APMI module, the applied force to the UAV $F_Z^{UAV} = K_{IGE}F_Z$ is different from the force commanded by the height controller F_Z, due to the ground effect K_{IGE}. When the APMI module is incorporated, the compensated control force F_Z is corrected to consider the increase due to the ground effect:

$$F_Z^{UAV} = K_{IGE}F_Z \qquad \text{without APMI module,} \quad (14a)$$

$$F_Z^{UAV} = K_{IGE}\underbrace{\frac{F_Z}{K_{IGE}}}_{\widehat{F_Z}} = F_Z \quad \text{with APMI module.} \quad (14b)$$

In this way, the force requested from the motors takes into account the increase due to ground effect, and now it matches that demanded by the height controller, as (14b) shows.

The proposed control scheme has been implemented modifying the Ardupilot autopilot.[1] As the APMI module is based on the proposed ground effect models, it needs only to evaluate the model expressions, requiring very low execution time. The execution time of these instructions has been measured on a Pixhawk board, obtaining an execution time lower than 10 μs. As the execution time is very small, the APMI module can be incorporated into the position control loop, which runs at 100 Hz in Ardupilot, without compromising its real-time execution. Fig. 7(a) shows the control architecture of the co-planar configuration with the APMI module, while Fig. 7(b) shows the control scheme for the fully-actuated platform.

B. Experimental Set-Up

The aerial platform for experimental validation is composed of the F550 frame which can be modified with 3D printed parts to tilt the motors and generate the fully-actuated configuration, as presented in Section II-A. The STL files of these 3D printed parts are available in our previous work [4]. The propulsive system of the aerial robot is composed of the DJI 2312E rotors, the DJI 9×4.5 propellers and the XRotor 40 A ESCs. All the system is powered by a 4S 5000mAh LiPo battery. The experimental validation is done for two configurations: the co-planar configuration and the fully-actuated configuration

[1]Code: https://github.com/antonio96agm/Ardupilot_IGE_APMI.git

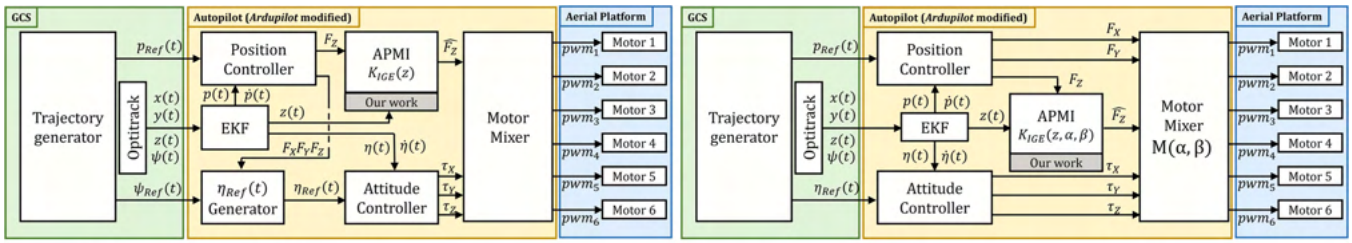

(a) Control scheme for the co-planar configuration

(b) Control scheme for the fully-actuated configuration

Fig. 7. Control scheme for experimental validation of the proposed model presented in Section III-A, for the co-planar configuration, and in Section III-B, for the fully-actuated configuration. The models are included as a correction in the APMI (Aerodynamic Power Model Inversion) module.

TABLE IV
RESULTS FOR THE DIFFERENT CONFIGURATIONS DURING THE FLIGHTS

Conf.	Controller	MAE	RMSE
Co-planar	w/ APMI	8.12 cm	3.43 cm
	w/o APMI	16.42 cm	6.77 cm
F. Actuated	w/ APMI	6.39 cm	3.13 cm
	w/o APMI	14.52 cm	6.65 cm

with $\alpha = \beta = 20°$. For each configuration, two flights where performed, one without the APMI module and another with the APMI module, doing a total of four flights.

To command a trajectory to the UAV, a Ground Control Station (GCS) is used to send the desired position and orientation via MAVLink. In addition, the position and yaw angle of the platform are measured by the Optitrack motion capture system. Optitrack data are streamed from the GCS to the aerial platform over WiFi connection. The autopilot EKF (Extended Kalman Filter) uses the Optitrack measurements to estimates the UAV position and velocity, allowing control the position of the platform.

In order to validate the models, the height error is compared both with the APMI module and without the APMI module, which applies a ground effect compensation into F_Z. Each model is validated with a flight that combines instants of low and high ground effect impact. During the flight the multirotor follows the trajectory $z_{Ref}(t) = 0.55 + 0.45cos(2\pi t/T)$, with $T = 5\ s$, where the impact of the ground effect is significant in the lower part of the reference. The GCS sends to the UAV the waypoints of the trajectory through the MAVLink protocol.

C. Results and Analysis

Two metrics were used to compare tracking error with and without IGE compensation: the maximum absolute error (MAE) and the root mean square error (RMSE). These metrics are computed as follows:

$$MAE = \max(|e_z(t)|) \quad RMSE = \sqrt{\frac{1}{t_T}\int_0^{t_T} e_z(\tau)d\tau}, \quad (15)$$

where t_T is the total duration of the experiment. Table IV presents these two metrics for the four experiments performed: co-planar configuration with the APMI (w/ APMI) module and without the APMI (w/o APMI) module, and fully-actuated configuration with the APMI module and without the APMI module.

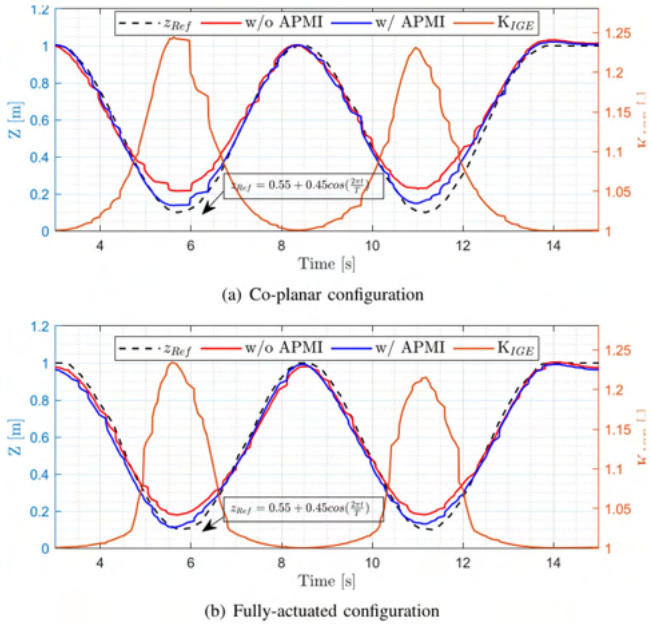

(a) Co-planar configuration

(b) Fully-actuated configuration

Fig. 8. Results of the co-planar and fully-actuated platforms during the experiments. The left axis shows the reference position (z_{Ref}) during the flights, the position during the experiment without the APMI module, and the position during the experiment with the APMI module. The right axis shows the correction factor K_{IGE} computed by the APMI module and applied only during the experiment with the APMI module.

1) Co-Planar Configuration: Fig. 8(a) presents the results with the co-planar configuration. It can be observed that as the platform approaches the ground, the tracking error increases if the APMI module is not used. However, using the APMI module reduces the tracking error near the ground, as it compensates for the additional thrust caused by the ground effect. In addition, as Table IV shows, the APMI module reduces up to 50% the MAE and the RMSE, leading to a more precise flight.

2) Fully-Actuated Configuration: Fig. 8(b) shows the results with the fully-actuated configuration. Similarly to the co-planar platform, the tracking error is reduced at the moments of high ground effect influence when using APMI module. In addition, as before, APMI module reduces up to 50% the MAE and the RMSE, as shown in Table IV.

Likewise, comparing the results obtained with the co-planar platform with those obtained with the fully-actuated platform, it is observed that the errors are higher in the co-planar configuration. This is due to the fact that, for the same height with

respect to the ground, the ground effect influence is greater in the co-planar configuration than in the fully-actuated configuration, as seen in Section III. In addition, this is observed in the applied correction factor K_{IGE} by the APMI module, which takes higher values in the co-planar configuration than in the fully-actuated configuration.

In summary, these experiments show that the incorporation of the proposed models in the control law by the APMI module considerably improves the accuracy of flights under the influence of ground effect. These results allow us to validate the proposed models not only in test-bench experiments but also in real flights.

V. Conclusion

This study proposes two different aerodynamic ground effect models, tailored for co-planar configurations and for platforms equipped with tilted rotors, respectively. A comprehensive series of experiments were executed, considering an array of rotor inclinations and UAV flight elevations. These semi-empirical models were further validated through a series of real indoor flights. With the emergence of the fully-actuated multirotor concept, previous models are not applicable because the rotor inclination is not considered. This work addresses this gap and gives an in-depth understanding of how tilt affects a UAV when approaching a surface.

The results reveal that the increase in thrust experienced by the UAV near the ground increases with tilt. However, the trend reverses as the UAVs move away from the ground. In this case, the ground effect is reduced as the inclination increases, similar to a single-inclined rotor. In general, the ground effect is lower for the tilted cases than for the co-planar case. After implementing the aerodynamic models into the UAV controller and executing indoor flights, there was a marked improvement in the hexarotor's precision and performance in reaching the desired position near the ground.

Acknowledgment

The authors would like to thank to Carlos Alvarez Cia, as member of GRVC, for his help during experimental flights.

References

[1] K. P. Valavanis and G. J. Vachtsevanos, *Handbook of Unmanned Aerial Vehicles*, vol. 2077. Berlin, Germany: Springer, 2015.

[2] A. Ollero et al., "The AEROARMS project: Aerial robots with advanced manipulation capabilities for inspection and maintenance," *IEEE Robot. Automat. Mag.*, vol. 25, no. 4, pp. 12–23, Dec. 2018.

[3] A. Praveen, X. Ma, H. Manoj, V. L. Venkatesh, M. Rastgaar, and R. M. Voyles, "Inspection-on-the-fly using hybrid physical interaction control for aerial manipulators," in *Proc. IEEE/RSJ Int. Conf. Intell. Robots Syst.*, 2020, pp. 1583–1588.

[4] P. J. Sanchez-Cuevas et al., "Fully-actuated aerial manipulator for infrastructure contact inspection: Design, modeling, localization, and control," *Sensors*, vol. 20, no. 17, 2020, Art. no. 4708.

[5] K. Bodie et al., "Active interaction force control for contact-based inspection with a fully actuated aerial vehicle," *IEEE Trans. Robot.*, vol. 37, no. 3, pp. 709–722, Jun. 2021.

[6] F. Ruggiero, V. Lippiello, and A. Ollero, "Aerial manipulation: A literature review," *IEEE Robot. Automat. Lett.*, vol. 3, no. 3, pp. 1957–1964, Jul. 2018.

[7] R. Mahony, V. Kumar, and P. Corke, "Multirotor aerial vehicles: Modeling, estimation, and control of quadrotor," *IEEE Robot. Automat. Mag.*, vol. 19, no. 3, pp. 20–32, Sep. 2012.

[8] A. E. Jimenez-Cano, P. J. Sanchez-Cuevas, P. Grau, A. Ollero, and G. Heredia, "Contact-based bridge inspection multirotors: Design, modeling, and control considering the ceiling effect," *IEEE Robot. Automat. Lett.*, vol. 4, no. 4, pp. 3561–3568, Oct. 2019.

[9] S. J. Lee, D. Lee, J. Kim, D. Kim, I. Jang, and H. J. Kim, "Fully actuated autonomous flight of thruster-tilting multirotor," *IEEE/ASME Trans. Mechatronics*, vol. 26, no. 2, pp. 765–776, Apr. 2021.

[10] R. Rashad, D. Bicego, R. Jiao, S. Sanchez-Escalonilla, and S. Stramigioli, "Towards vision-based impedance control for the contact inspection of unknown generically-shaped surfaces with a fully-actuated UAV," in *Proc. IEEE/RSJ Int. Conf. Intell. Robots Syst.*, 2020, pp. 1605–1612.

[11] A. González-Morgado, C. Álvarez Cía, G. Heredia, and A. Ollero, "Fully-actuated, corner contact aerial robot for inspection of hard-to-reach bridge areas," in *Proc. IEEE Int. Conf. Unmanned Aircr. Syst.*, 2023, pp. 1191–1198.

[12] C. Powers, D. Mellinger, A. Kushleyev, B. Kothmann, and V. Kumar, *Influence of Aerodynamics and Proximity Effects in Quadrotor Flight*. Cham, Germany: Springer Int. Publishing, 2013, pp. 289–302.

[13] V. Britcher and S. Bergbreiter, "Use of a MEMS differential pressure sensor to detect ground, ceiling, and walls on small quadrotors," *IEEE Robot. Automat. Lett.*, vol. 6, no. 3, pp. 4568–4575, Jul. 2021.

[14] X. Kan, J. Thomas, H. Teng, H. G. Tanner, V. Kumar, and K. Karydis, "Analysis of ground effect for small-scale UAVs in forward flight," *IEEE Robot. Automat. Lett.*, vol. 4, no. 4, pp. 3860–3867, Oct. 2019.

[15] P. Sanchez-Cuevas, G. Heredia, and A. Ollero, "Characterization of the aerodynamic ground effect and its influence in multirotor control," *Int. J. Aerosp. Eng.*, vol. 217, pp. 1–17, 2017.

[16] P. Abbaraju, X. Ma, G. Jiang, M. Rastgaar, and R. M. Voyles, "Aerodynamic modeling of fully-actuated multirotor UAVs with nonparallel actuators," in *Proc. IEEE/RSJ Int. Conf. Intell. Robots Syst.*, 2021, pp. 9639–9645.

[17] C. Li, C. Xue, and Y. Bai, "Experimental investigation on aerodynamics of nonplanar rotor pairs in a multi-rotor UAV," in *Proc. 14th IEEE Conf. Ind. Electron. Appl.*, 2019, pp. 911–915.

[18] A. Garofano-Soldado, G. Heredia, and A. Ollero, "Aerodynamic interactions of non-planar rotor pairs and model derivation in ground approach," *Aerosp. Sci. Technol.*, vol. 142, 2023, Art. no. 108672.

[19] I. Cheeseman and W. Bennett, "The effect of ground on a helicopter rotor in forward flight," *ARC R M 3021*, 1955.

[20] A. Matus-Vargas, G. Gamez, and J. Martinez-Carranza, "Ground effect on rotorcraft unmanned aerial vehicles: A review," *Intell. Service Robot.*, vol. 14, pp. 1–20, 2021.

[21] A. Garofano-Soldado, P. J. Sanchez-Cuevas, G. Heredia, and A. Ollero, "Numerical-experimental evaluation and modelling of aerodynamic ground effect for small-scale tilted propellers at low Reynolds numbers," *Aerosp. Sci. Technol.*, vol. 126, 2022, Art. no. 107625.

[22] S. Rajappa, M. Ryll, H. H. Bülthoff, and A. Franchi, "Modeling, control and design optimization for a fully-actuated hexarotor aerial vehicle with tilted propellers," in *Proc. IEEE Int. Conf. Robot. Automat.*, 2015, pp. 4006–4013.

[23] S. A. Conyers, M. J. Rutherford, and K. P. Valavanis, "An empirical evaluation of ground effect for small-scale rotorcraft," in *Proc. IEEE Int. Conf. Robot. Automat.*, 2018, pp. 1244–1250.

[24] R. W. Deters, G. K. A. Krishnan, and M. S. Selig, "Reynolds number effects on the performance of small-scale propellers," in *32nd AIAA Appl. Aerodynamics Conf.*, 2014.